NeuroImage 332 (2026) 121888

Contents lists available at ScienceDirect

NeuroImage

journal homepage: www.elsevier.com/locate/ynimg

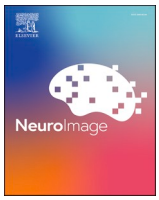

Enhanced default mode network stability in highly superior autobiographical memory

Fabrizio Parente [a,b,*], Tiziana Pedale [b,c], Ilenia Salsano [b], Patrizia Campolongo [a,d], Valerio Santangelo [b,c,*]

[a] Department of Physiology and Pharmacology, Sapienza University of Rome, P.le A. Moro 5, Rome 00185, Italy
[b] Functional Neuroimaging Laboratory, Fondazione Santa Lucia, IRCCS, Via Ardeatina 306, Rome 00179, Italy
[c] Department of Philosophy, Social Sciences & Education, University of Perugia, Piazza G. Ermini 1, Perugia 06123, Italy
[d] Neuropharmacology Unit, IRCCS Fondazione Santa Lucia, IRCCS, Via Ardeatina 306, Rome 00179, Italy

ARTICLE INFO

Keywords:
Autobiographical memory
Resting state
Default mode network
Dynamic and functional connectivity
Network analysis

ABSTRACT

The Default Mode Network (DMN) is a large-scale intrinsic brain network critically involved in internally oriented cognition, including autobiographical memory. Core DMN regions such as the hippocampus and medial prefrontal cortex are central to memory retrieval, schema construction and self-referential processing. Individuals with Highly Superior Autobiographical Memory (HSAM) provide a unique model to investigate the neural mechanisms underlying exceptional memory ability. However, the intrinsic functional connectivity and temporal dynamics of the DMN in HSAM remain largely unexplored. To provide new insight into the baseline network mechanisms that supports HSAM irrespective of memory retrieval, in this study we examined both static and dynamic features of DMN functional architecture in 12 HSAM individuals and 31 matched controls during resting-state fMRI. Using a multilevel analytical framework encompassing link-level, node-level, and whole-network level measures, we characterized connectivity strength, temporal variability, and co-activation dynamics within the DMN. HSAM individuals showed enhanced and more temporally stable functional connectivity among memory-related, schema-related, and self-referential DMN regions, including the hippocampus, temporal pole, and ventromedial prefrontal cortex. These findings suggest that HSAM is associated with a more integrated and stable DMN organization, potentially supporting continuous memory replay and the consolidation of autobiographical experiences. This enhanced DMN coherence may represent a neural signature of HSAM.

1. Introduction

The Default Mode Network (DMN) is a large-scale intrinsic brain network encompassing midline and temporo-parietal regions, characterized by enhanced intra-network functional connectivity (FC) during the resting state (Raichle et al., 2001; Raichle and Snyder, 2007; Greicius et al., 2009; Andrews-Hanna et al., 2014a; Andrews-Hanna et al., 2014b). According to the model proposed by Andrews-Hanna et al. (2014a), the core system of the DMN comprises the medial prefrontal cortex (mPFC) and the posterior cingulate cortex (PCC), which interact with two additional DMN subsystems: the medial temporal subsystem, including the hippocampus (HC), the parahippocampus (PHC), and the ventromedial PFC (vmPFC); and the dorsal medial subsystem, centred on the dorsomedial PFC (dmPFC) and extending to lateral regions such as the temporoparietal junction (TPJ) and the lateral parieto-temporal cortex. The DMN was initially described as a task-negative network, showing reduced activity during externally demanding tasks (Raichle et al., 2001). However, it has since been shown to support a wide range of internally directed cognitive processes, including mind-wandering (Zhou and Lei, 2018; Kim and Lee, 2022), mental simulation (Buckner and Carroll, 2007; Spreng et al., 2009; Hassabis and Maguire, 2009), episodic memory reactivation (Kaefer et al., 2022), semantic retrieval (Binder and Desai, 2011), and autobiographical memory (Bellana et al., 2017). Consistent with this broad functional involvement, Menon (2019) suggested that the DMN contributes to regulating the balance between internally and externally oriented attention through its interactions with other large-scale networks, such as the Salience Network and the Central Executive Network.

The link between the DMN and memory is particularly robust, as medial temporal and prefrontal regions within the DMN are key

* Corresponding authors at: Functional Neuroimaging Laboratory, IRCCS Santa Lucia, Via Ardeatina, 306 00179, Rome, Italy.
E-mail addresses: fabrizio.parente86@gmail.com (F. Parente), valerio.santangelo@unipg.it (V. Santangelo).

https://doi.org/10.1016/j.neuroimage.2026.121888
Received 31 December 2025; Received in revised form 9 March 2026; Accepted 24 March 2026
Available online 25 March 2026

substrates of episodic and autobiographical memory (Buzsáki and Moser, 2013; Daviddi et al., 2023, 2024; Nadel, 2013; Maguire and Mullally, 2013; Rolls, 2022; Moscovitch et al., 2016), supporting both the integration of past experiences and the retrieval of contextual details (Moscovitch et al., 2016; Sekeres et al., 2018). Recent work has proposed that the DMN may facilitate spontaneous memory reactivation, a mechanism considered crucial for consolidation (Kaefer et al., 2022). Given this central role in memory function, the DMN is a relevant target for investigating individuals with altered or exceptional memory abilities. In this context, individuals with HSAM (Parker et al., 2006; LePort et al., 2012) provide a unique opportunity to investigate memory-related neural circuits from a complementary perspective to clinical memory impairment (Santangelo et al., 2022). Individuals with HSAM can vividly and accurately retrieve remote autobiographical experiences without relying on explicit mnemonic strategies (Palombo et al., 2018; Talbot et al., 2025), while their performance in other cognitive domains remains largely unaffected (LePort et al., 2017; Daviddi et al., 2022a; Santangelo et al., 2025). Indeed, previous literature has revealed no significant differences between HSAM and control participants in non-autobiographical memory domains. For example, HSAM individuals do not outperform control participants in episodic or working memory tasks (LePort et al., 2012, 2017), attention and executive functions (LePort et al., 2017), creative thinking (Daviddi et al., 2022a), constructing future events from a third-person perspective (Gibson et al., 2022), or directed forgetting (Santangelo et al., 2025). HSAM individuals are also equally susceptible to false memories (Patihis et al., 2013) and only demonstrate an advantage for semantic information when it is personally relevant (Ford et al., 2022). Overall, the literature consistently highlights that the HSAM advantage is highly selective, being limited specifically to autobiographical memory.

Previous research has examined structural (Ally et al., 2013; Brandt and Bakker, 2018; Mazzoni et al., 2019; LePort et al., 2012; Ford et al., 2022; Gibson et al., 2022; Santangelo et al., 2021) and functional (Ally et al., 2013; Brandt and Bakker, 2018; Santangelo et al., 2018, 2020, 2021, 2025; Mazzoni et al., 2019; De Marco et al., 2021; Daviddi et al., 2022b; Orwig et al., 2024) correlates of HSAM. Structurally, altered fractional anisotropy (FA) in the left uncinate fasciculus has been reported (LePort et al., 2012), while task-based functional studies have shown increased activation during autobiographical memory retrieval in antero-medial (Santangelo et al., 2018, 2020, 2021) and posterior parietal regions (Mazzoni et al., 2019). Resting-state fMRI studies have expanded these findings: Orwig et al. (2024) reported increased connectivity between mPFC and PCC, suggesting a more integrated anteroposterior DMN axis, while De Marco et al. (2021) described widespread increases in large-scale connectivity in a single HSAM participant. Conversely, Daviddi et al. (2022b) found reduced hippocampal connectivity with the salience network and ventral attention network (VAN), along with increased connectivity with sensory regions — interpreted as reduced filtering of episodic details during encoding and consolidation process. Together, these findings suggest that HSAM may be characterized by reduced cross-network communication and enhanced within-DMN integration at rest (Daviddi et al., 2022b; Orwig et al., 2024; see also De Marco et al., 2021 for a single case study).

Given the DMN's central role in memory consolidation (Kaefer et al., 2022) and self-referential cognition (Buzsáki and Moser, 2013; Moscovitch et al., 2016), as well as the initial findings of enhanced within-DMN integration at rest in HSAM (De Marco et al., 2021; Daviddi et al., 2022b; Orwig et al., 2024), the present study further explored both the static and dynamic properties of resting-state DMN connectivity in HSAM vs. control participants. While previous resting-state studies in HSAM have used either seed-based approach (Daviddi et al., 2022b) or whole-brain approach (Orwig et al., 2024), here we aimed to focus specifically on the DMN organization. This approach was expected to corroborate task-based evidence which has consistently shown enhanced activations related to memory retrieval in HSAM (Ally et al., 2013; Mazzoni et al., 2019; Santangelo et al., 2018, 2020, 2021, 2025). Clarifying whether individuals with HSAM exhibit distinctive DMN connectivity patterns at rest, independent of any task demand, could provide insight into the baseline network mechanisms that support continuous autobiographical, self-referential processing and memory consolidation in HSAM. Using a multivariate approach (McIntosh and Lobaugh, 2004; Krishnan et al. 2011), we assessed not only the strength but also the temporal stability of DMN interactions in a resting-state fMRI (rsfMRI) dataset comprising 12 HSAM individuals and 31 matched controls. We hypothesized that HSAM participants would exhibit (1) increased pairwise FC among the 20 DMN nodes defined by Andrews-Hanna et al. (2014a) and (2) increased node-level centrality, assessed using a network-based approach (Rubinov and Sporns, 2010; Borgatti and Everett, 2006). Additionally, dynamic FC analyses using Temporal Variability (TV; Zhang et al., 2016) and Co-Activation Patterns (CAPs; Liu et al., 2013; Chen et al., 2015) allowed us to examine the temporal stability and dynamic reconfiguration of DMN activity (Long et al., 2023). This approach aims to clarify the dynamic neural architecture of DMN supporting HSAM.

2. Methods

2.1. Participants

The study included 12 individuals with HSAM (3 females; mean age 35.3, range: 20-60 years) and 31 control (i.e., normal memory) subjects (13 females; mean age 35.9 years, range: 21-59 years). HSAM individuals constitute an extremely rare population, and the present sample size is consistent with, or larger than, that of prior neuroimaging studies which relied on single-case investigations (e.g. Ally et al., 2013; Brandt and Bakker, 2018; Mazzoni et al., 2019; Gibson et al., 2022), or similar cohorts (e.g. LePort et al., 2012; Santangelo et al., 2020; 2025). To improve statistical stability and the precision of baseline estimates, the size of the control group was more than doubled relative to the HSAM group.

Participants with HSAM have been screened using the procedure previously described by LePort et al. (2012) and adapted for the Italian population (Santangelo et al. 2018). The screening process involved administering two standardized tests: the Public Events Quiz and the Random Dates Quiz (LePort et al., 2012). The Public Events Quiz comprised 30 questions covering five categories of public events: sporting events, political events, notable negative events, events related to famous individuals, and holidays. Half of the questions required participants to recall the exact date of a specific public event, while the other half asked participants to identify a significant public event that occurred on a given date. The Random Dates Quiz included 10 computer-generated dates ranging from the participant's 15th year to the day before the test. For each date, participants were asked to provide three details: (1) the day of the week, (2) a verifiable event occurring within one month before or after the date, and (3) a personal autobiographical event. The current HSAM sample achieved a mean accuracy of 55% on the Public Events Quiz and 65% on the Random Dates Quiz, which was consistent with previous literature. None of the control participants reported having HSAM or any other superior memory abilities (for a similar approach, see LePort et al., 2012). The two groups were matched for age and education [both using a two-tailed independent-sample t-test: p-value > 0.05]. All participants had normal or corrected-to-normal (with contact lenses) visual acuity. The participants received an explanation of the procedures and gave written informed consent. The study was approved by the independent Ethics Committee of Fondazione Santa Lucia, IRCCS, and conducted in adherence to the tenets of the Declaration of Helsinki.

2.2. Image acquisition, fMRI data preprocessing

Functional images in a resting state condition were acquired using a Siemens Prisma (Siemens Medical Systems, Erlangen, Germany)

operating at 3T and equipped for simultaneous multi-slice echo-planar imaging (EPI). A quadrature volume head coil was used for radio frequency transmission and reception. Head movement was minimized by mild restraint and cushioning. During the resting-state scan, participants were instructed to rest with their eyes open, fixating on a central cross, and to allow their thoughts to flow freely without engaging in any structured mental activity. They were asked to remain still and to avoid falling asleep. Instructions were provided prior to scanner entry. Head motion was monitored online throughout data acquisition by the operators. After each scanning run, participants were asked to provide feedback to confirm compliance with the instructions. Functional images were acquired using blood oxygenation level–dependent (BOLD) contrast with the following parameters: 322 volumes acquired over 6 min; voxel size = 2.4 × 2.4 × 2.4 mm^3; distance factor = 0%; repetition time (TR) = 1.1 s; echo time (TE) = 33 ms; 60 axial slices. Before the fMRI runs, a structural image was collected using a T1-weighted MPRAGE sequence (TR = 2.5 s, TE = 2 ms, flip angle = 8°, FOV = 256 × 256 mm; slice thickness = 1 mm).

The first four scans were deleted, after which a standard preprocessing pipeline involving indirect normalization to MNI space was carried out. This included functional realignment and unwarping, slice timing correction, functional and structural normalization, structural segmentation, and smoothing (8 mm). ART-based outlier detection (Power et al., 2014) was then used to identify movement-related outliers (framewise displacement > 0.9 mm and global signal changes > 5 S.D.). The motion parameters (12 components) were subsequently regressed out. In the denoising step, a band-pass filter (range: 0.008 – 0.09 Hz) was applied and the anatomical CompCorr method (Behzadi et al., 2007) was used to correct the functional images for noise components from white matter (WM, five components) and cerebrospinal fluid (CSF, five components).

The main aim of the current study was to compare the activity of the DMN in individuals with HSAM vs. control subjects at rest. Based on the studies of Andrews-Hanna et al. (2010) and Bellana et al. (2017), 20 Regions of Interest (ROIs) were used to characterize the DMN (see Table 1). MarsBar toolbox (https://marsbar-toolbox.github.io/) was used to build 8-mm spheres at the coordinates of the ROIs that were used as masks for the extraction of the timeseries. The BOLD timeseries were extracted from all the voxels within each ROI and averaged to calculate the meantime courses. The previous operations were performed using SPM12 (Statistical Parametring Mapping, Wellcome Department of Cognitive Neurology, London, UK) and The CONN toolbox version 18b (Whitfield-Gabrieli and Nieto-Castanon, 2012) on a MatLab R2018a platform.

Table 1
MNI coordinates of ROIs characterizing the DMN based on Andrews-Hanna et al. (2010) and Bellana et al. (2017).

Regions (abbreviation)	x	y	z
Left Hippocampus (HC)	-22	-20	-26
Right Hippocampus	22	-20	-26
Left Parahippocampus (PHC)	-28	-40	-12
Right Parahippocampus	28	-40	-12
Left Retrosplenial Cortex (RSP)	-14	-52	8
Right Retrosplenial Cortex	14	-52	8
Ventromedial prefrontal cortex (vmPFC)	0	26	-18
Dorsomedial prefrontal cortex (dmPFC)	0	52	26
Left anterior medial prefrontal cortex (amPFC)	-6	52	-2
Right anterior medial prefrontal cortex	6	52	-2
Left Temporal Pole (TempP)	-50	14	-40
Right Temporal Pole	50	14	-40
Left Lateral Temporal Cortex (LTC)	-60	-24	-18
Right Lateral Temporal Cortex	60	-24	-18
Left Temporoparietal Junction (TPJ)	-54	-54	28
Right Temporoparietal Junction	54	-54	28
Left Posterior Cingulate Cortex (PCC)	-8	-56	26
Right Posterior Cingulate Cortex	8	-56	26
Left Posterior Inferior Parietal Lobule (pIPL)	-44	-74	32
Right Posterior Inferior Parietal Lobule	44	74	32

2.3. Analysis

To characterize the connectivity of the DMN, a three-level approach involving the following has been used: (1) a single-link analysis using multivariate approach of FC patterns; (2) a single-node analysis (i.e., a brain region analysis) characterizing the strength and the temporal variability for each brain region; and (3) a whole-network analysis that estimates dynamic properties using the co-activation pattern method. The analyses were conducted using the Brain Connectivity Toolbox (BCT; https://sites.google.com/site/bctnet/; Rubinov and Sporn, 2010) and a custom-made script on the Matlab platform (R2018b).

2.3.1. Single-link analysis: functional connectivity and multivariate analysis

For the first analysis, the FC was calculated as a Pearson correlation (r) between the timeseries of the 20 ROIs. Correlation values were then transformed in the Fisher's Z score according to the following formula [0.5 * ln((1+r)/(1-r))], resulting in a squared and symmetric matrix for each participant, i.e., the adjacency matrix. A mean-centred Partial Least Square Correlation (PLSC) analysis was performed to characterize the functional measures pattern related to each group. PLSC is a data-driven multivariate analysis based on the singular value decomposition (SVD) of a cross-product matrix (R) generated by the product between a data matrix (X) and a contrast matrix (Y) (see, for a complete description of the procedure, McIntosh and Lobaugh, 2004; Krishnan et al. 2011). Following the approach of Bellana et al. (2017), the *X* matrix was set as the 190 unique functional connectivity values (Fisher-Z transformed) derived by the cross-correlations among the 20 ROIs of the DMN (i.e., [20*(20-1)/2]), and including subjects of both groups (size matrix: 43 × 190; 12 HSAM + 31 controls= 43 total subjects). Then, we characterized the dummy coded contrast matrix *Y* differentiating groups (HSAM and control subjects) for each connectivity pattern. This procedure allowed us to detect a set of Latent Variables (LVs) that identifies how the pattern of the functional measures varied across groups. The salience attributed to the explanatory variables (HSAM and control subjects) describes the relation between them and the corresponding LV, allowing us to detect a given patterns of values related to the original variables. Thus, pattern with positive saliences on a particular LV are related to a given set of explanatory variables having positive saliences, otherwise connectivity with negative saliences is related to those explanatory variables having negative saliences. It is important to emphasize that the direction of the saliences (positive vs. negative) is arbitrary. Connections with positive saliences are those that are more characteristic of one group, while those with negative saliences are those that are more characteristic of the other group. Therefore, the distinction is related to groups rather than being an absolute measure of an increase or decrease in connectivity. To estimate the p-value associated to the results, a permutation test was performed (McIntosh and Lobaugh, 2004). Observations in the data matrix X were randomly reordered (bootstrapping without replacement) and the PLSC analysis was repeated for 1000 times. The set of the singular values obtained was defined as the distribution of the null hypothesis and used to estimate the probability value (p-value < 0.05). To calculate the confidence interval (CI) and standard error, a new

re-sample of both *X* and *Y* matrices was computed using a bootstrap with replacement method. The bootstrap ratio was used to check the stability of the results and their generalizability to the population (i.e., a random effect model) (McIntosh and Lobaugh, 2004; Efron and Tibshirani, 1986).

2.3.2. Single-node analysis: node strength and temporal variability

To explore other functional and dynamical characteristic of the DMN a network theory approach was used (Rubinov and Sporn, 2010). Single nodes (i.e., brain regions) belonging to the functional brain network were studied by two different points of view: strength (Borgatti and Everett, 2006) and TV (Zhang et al., 2016).

In a network theory approach, the interactions of a given node within the entire network are estimated using the node strength (Borgatti and Everett, 2006). Node strength was calculated by summing the set of functional connectivity values (weight links) of each brain region (i.e. each of the 20 nodes) to the other 19 nodes, using the previously described adjacency matrix. This measure accounts for the interactions of a given node within the network (Borgatti and Everett, 2006). However, since negative values of functional connectivity are difficult to interpret (Murphy et al., 2009; Fox et al., 2009; Chang and Glover, 2009; Chai et al., 2012; Gopinath et al., 2015; Parente and Colosimo, 2020), only the positive values were used, with the negative values being set to 0.

TV analysis was used to estimate temporal changes in FC, capturing the variability of each node's connectivity across the acquisition time (Zhang et al., 2016). This measure is derived from the BOLD time series to quantify how FC patterns differ over time. Traditionally, TV is computed by segmenting the BOLD signal into *n* non-overlapping windows of length *l*. However, to avoid the arbitrary choice of window size, we employed the edge time-series (eTS) approach (Betzel et al., 2023). Using eTS, for each pair of nodes (*X, Y*), a co-fluctuating time-series is obtained as: $r_{x,y}= [x_1*y_1, \ldots, x_t*y_t]$, where x_t corresponds to the z-score transformed BOLD values of the region *x* at the time *t*. This yields a parameter-free approach that does not require windowing. The FC profile of region *a* at time window *t* is then represented as the vector $F_{t,a}$, reflecting the set of functional connections of region *a* at that moment. Then, for each pair of windows, the Pearson correlation coefficient between the corresponding FC profiles ($F_{t1,a}$,$F_{t2,a}$), was calculated, and a correlation distance measure obtained as: $V_a= 1-$ corrcoef($F_{t1,a}$,$F_{t2,a}$). The TV index of region *a* was calculated as the average of these correlation distance values across all pairs of windows. Higher values indicate greater fluctuation in the connectivity profile of the region over time, reflecting reduced temporal stability and greater dynamic reconfiguration of its functional interactions.

Two independent multivariate analyses were performed for both nodes' measures. As in the previous analysis (see paragraph 2.3.1), a mean-centred PLSC analysis was performed to characterize the functional patterns associated with each group. In the first analysis, the *X* matrix was created using the node strength of each subject, resulting in a 43 × 20 data matrix. In the second analysis, the *X* matrix contained the TV values that characterized each brain region, resulting again in a 43 × 20 data matrix. Then, we characterized the dummy coded contrast matrix *Y* differentiating groups (HSAM and control subjects) for each strength and TV pattern, separately. As previously described, p-values, CIs, and standard errors were estimated using a permutation test (McIntosh and Lobaugh, 2004). Specifically, the permutation test was run 1000 times with bootstrap resampling applied to generate the sampling distributions: without replacement for the permutation step, and with replacement for the estimation of CIs and standard errors (McIntosh and Lobaugh, 2004; Efron and Tibshirani, 1986).

2.3.3. Whole-network analysis: dynamical characterization by the Co-activation pattern (CAP) analysis

Finally, we conducted a CAP analysis (Liu et al. 2013; 2018a), which allowed us to characterize possible connectivity patterns and describe time-changing brain states across the scans. Compared to other dynamic approaches (e.g., sliding window, temporal ICA, etc.), CAP analysis enables estimation of brain state sequences closer to the minimum temporal resolution (i.e., each scan), requiring very few assumptions about the model. This procedure considers the particular combination of positive and negative BOLD signal values estimated for each scan acquisition. To avoid noise and minor signal acquisition perturbations (Shmuel et al., 2002; Taylor et al., 2022), positive and negative values were selected using an asymmetric threshold, excluding scans with transformed z-score values within the range [1.5, -2]. The resulting measures were concatenated to produce a single matrix containing all the activations and deactivations of the entire dataset, including both HSAM individuals and control subjects. Subsequently, the k-means procedure was used to group each scan into a defined number of connectivity patterns, describing the possible brain states during acquisition. The Caliński-Harabasz approach was used to evaluate the number of clusters (Caliński and Harabasz, 1974). Next, the sequence of brain states for each subject was reconstructed and the dynamic metrics were calculated. The following indices were estimated: occurrence rate, dwell time, and transition matrix. The first index calculates the proportion of time that each brain cluster is present during the scan; the second estimates the average duration of a continuous brain state; and the third describes the transition probability between each brain state using the recurrence matrix. Statistical analyses were performed differently. For the first two indices (occurrence rate and dwell time), a series of non-parametric statistical comparisons were performed between the groups using the Wilcoxon signed-rank test. Mean-centred PCLS analysis was performed on the estimated transition matrix. As for the previous analysis, the matrix *X* was defined in terms of the probability value of the transition matrix (43 × 9), while the dummy-coded contrast matrix *Y* was set to differentiate the groups (HSAM vs. control subjects).

3. Results

3.1. Single-link analysis: functional connectivity

Mean-centred PLSC analysis revealed a main Latent Variable (LV) that describes the differences between the groups. Fig. 1 (Panel A) illustrates the salience associated with each group: positive salience is associated with the FC of the control group, while negative salience is associated with the FC of the HSAM group.

Panel B of Fig. 1 shows the spatial distribution of the FC. Table 2 reports the specific FC characterized by significant saliences related to the HSAM and control groups.

HSAM subjects showed increased FC between the posterior and the anterior parts of the DMN. HC, PHC and RSP exhibited increased connectivity to various regions of the prefrontal cortex, including the anterior medial, dorsomedial and ventromedial regions. The HSAM group exhibited an additional pattern of increased connectivity involving different regions within the posterior part of the DMN, including the HC, PHC, LTC, pIPL and RSP. Only FC between the left and right amPFC was reduced in the HSAM compared to the control group.

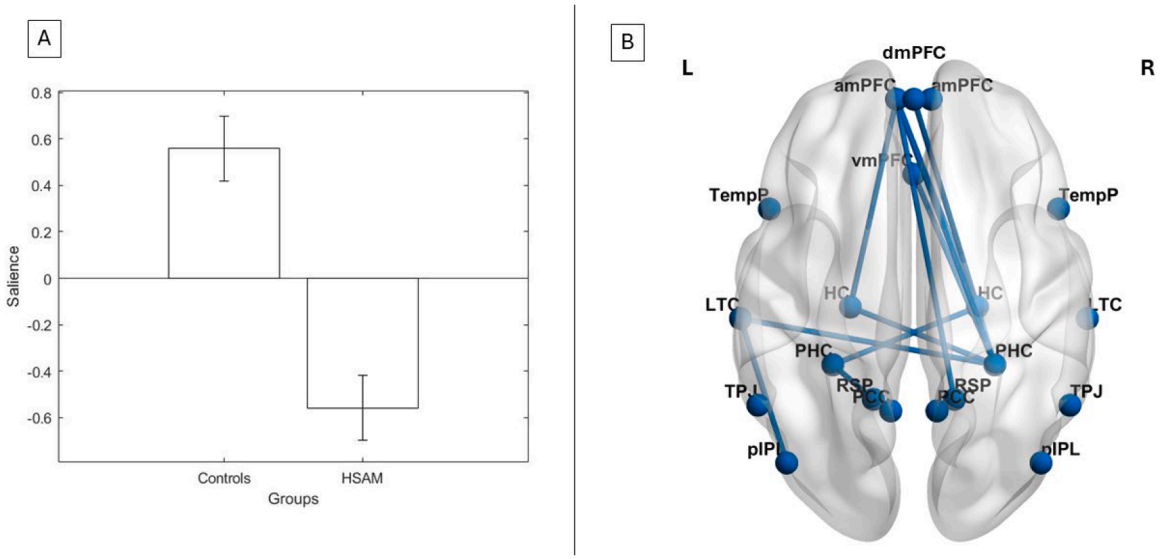

Fig. 1. Saliences of the main Latent Variable (LV), characterized by an opposite pattern of FC between the groups at rest. Positive and negative saliences were associated with the control group and the HSAM group, respectively. Panel A: saliences of the explanatory variables; error bars represent 95% CIs. Panel B: axial brain representation of the FC pattern characterizing the HSAM group; edges indicate connections that are increased in HSAM subjects.

Table 2
Connectivity and salience values associated to positive and negative values of to the first LV.

Connections	LV1 (positive)			LV1 (negative)			
	FC (Mean ± std)		Salience (Mean ± std)	Connections	FC (Mean ± std)		Salience (Mean ± std)
	HSAM	Controls			HSAM	Controls	
amPFC left – amPFC right	0.97 ± 0.26	1.16 ± 0.28	0.14 ± 0.06	HC left – PHC right	0.34 ± 0.15	0.22 ± 0.16	-0.08 ± 0.04
				HC left – amPFC left	0.27 ± 0.12	0.17 ± 0.20	-0.07 ± 0.04
				HC right – PHC left	0.44 ± 0.22	0.24 ± 0.20	-0.15 ± 0.05
				HC right – PHC right	0.39 ± 0.19	0.26 ± 0.17	-0.10 ± 0.04
				HC right – amPFC left	0.25 ± 0.17	0.10 ± 0.19	-0.11 ± 0.04
				HC right - dmPFC	0.14 ± 0.17	0.02 ± 0.21	-0.09 ± 0.04
				LTC left – PHC right	0.09 ± 0.16	-0.02 ± 0.18	-0.08 ± 0.04
				LTC left – pIPL left	0.48 ± 0.21	0.29 ± 0.25	-0.14 ± 0.05
				PHC left – RSP left	0.79 ± 0.25	0.24 ± 0.20	-0.12 ± 0.06
				PHC right – amPFC left	0.24 ± 0.14	0.62 ± 0.25	-0.13 ± 0.04
				PHC right – vmPFC	0.20 ± 0.21	0.06 ± 0.21	-0.10 ± 0.05
				RSP right – amPFC left	0.40 ± 0.17	0.06 ± 0.19	-0.10 ± 0.04

Left column and right column are related to positive and negative salience of the first LV, respectively. Positive salience is associated to increased FC in controls; negative salience is associated to increased FC in HSAM group. Only the significant saliences after a bootstrapping method are shown. amPFC: anterior medial prefrontal cortex; HC: hippocampus; PHC: parahippocampus; amPFC: anterior medial prefrontal cortex; dmPFC: dorsomedial prefrontal cortex; LTC: lateral temporal cortex; pIPL: posterior inferior parietal lobule; RSP: restrosplenial cortex; vmPFC: ventromedial prefrontal cortex.

3.2. Single-node analysis

3.2.1. Node strength

Fig. 2 (panel A) illustrates the salience associated with the first LV. The analysis revealed a significant effect of group. Panel B shows the vector of the nodes, which specifies the set of brain regions associated with the positive (controls) and negative (HSAM) salience. Two brain regions were found to be associated with the HSAM group: the right HC and PHC. These regions were found to be more connected to the rest of the network in the HSAM group, as highlighted in Table 3. No significant node strength was found in the control group.

3.2.2. Temporal variability (TV)

The first LV was characterized by negative and positive salience, which was associated with an increased TV in the control group compared to the HSAM group (Fig. 3, panel A). The single node analysis (panel B) revealed a decreased variability values in the right HC and left TempP in the HSAM group (see Table 4).

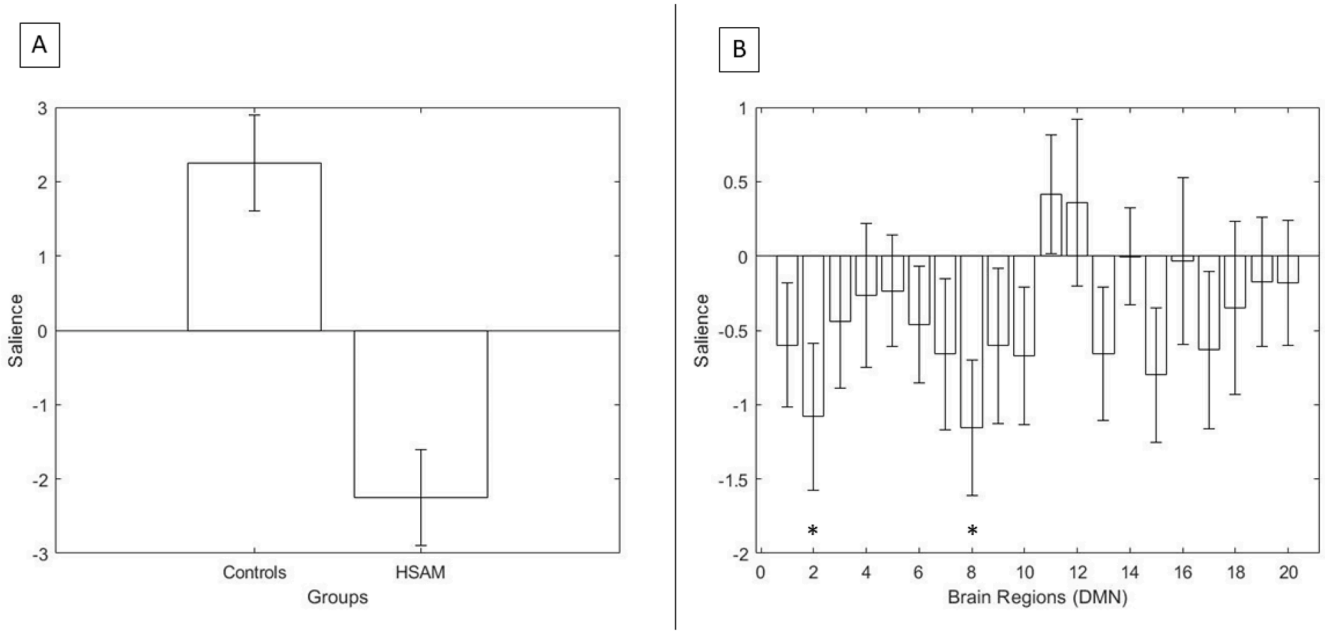

Fig. 2. Saliences of the main Latent Variable (LV), which characterizes an opposite pattern of node strength between groups. Positive and negative saliences were associated with the control and HSAM group, respectively. Panel A: saliences of explanatory variables; Panel B: node strength vectors of salience related to each brain region; asterisks indicate significant salience after the permutation test. Error bars represent 95% CIs.

Table 3
Node strength and salience of the brain regions related to the HSAM group (first LV, negative salience). No significant results were found in relation to the positive salience in the first LV.

Brain Regions	LV1 (negative)		
	Node strength (Mean ± std)		Salience (Mean ± std)
	HSAM	Controls	
HC right	5.1 ± 2.2	3.6 ± 2.0	-1.080 ± 0.495
PHC right	5.4 ± 1.9	3.8 ± 2.0	-1.154 ± 0.454

Left column: node strength of HSAM group; right column: node strength of controls. Only significant saliences after the bootstrapping are shown. HC: hippocampus; PHC: parahippocampus.

3.3. Whole-network analysis: Co-activation pattern (CAP)

Using the Caliński–Harabasz criterion (Caliński and Harabasz, 1974), three clusters were identified across scans, corresponding to three distinct brain states that characterized the entire dataset, including both HSAM and control subjects (see Fig. 4 and Table 5). The first cluster comprises bilateral brain regions mainly belonging to the dorsal medial subsystem of the DMN (dmPFC, LTC, TPJ and TempP), as well as the central core (amPFC and PCC). The second cluster comprises brain regions mainly belonging to the medial temporal subsystem (HC, PHC, RSP, pIPL and vmPFC), the central core hub (PCC) and a right-lateralized part of the dorsal medial subsystem (LTC and TPJ). The third cluster comprised brain regions belonging to both subsystem (TempP, HC and vmPFC).

Statistical analysis of the occurrence rate and dwell time shows no significant differences between groups for each cluster (Fig. 5, left and right panels, and Table 6). Finally, the transition matrix was estimated (Fig. 6), and PLSC analysis was performed on the transition probability values between brain states and between groups. Fig. 7 illustrates the significant group effect associated with positive and negative values for the control and HSAM groups, respectively. Panel B shows an increase in transition probabilities from state 3 to 2 in the control group, and from state 3 to 3 in the HSAM group.

4. Discussion

In this study, we used a multilevel approach to investigate static and dynamic properties of DMN functional architecture in individuals with

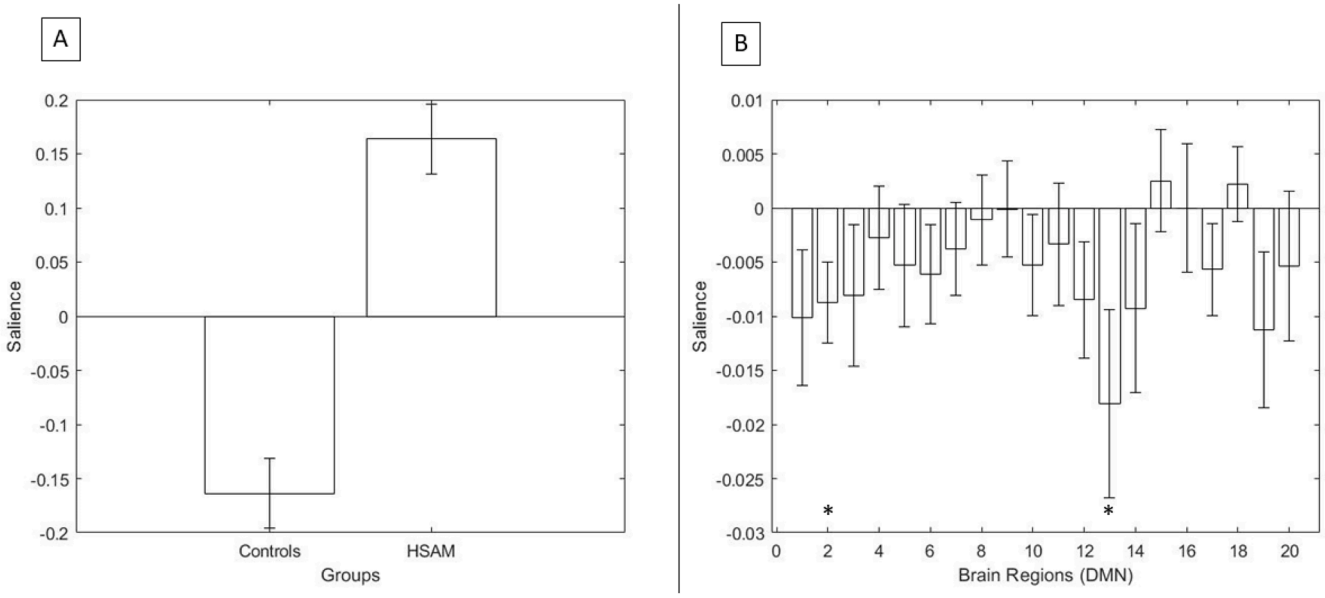

Fig. 3. Saliences of the main Latent Variable (LV), which characterizes an opposite pattern of TV values between groups. Positive and negative saliences were associated with the HSAM and control group, respectively. Panel A: saliences of explanatory variables; Panel B: TV vectors of salience related to each brain region. Asterisks indicate significant salience after the permutation test. Error bars represent 95% CIs.

Table 4
Brain regions with a decreased TV in the HSAM group (i.e., increased values in the control group). Only brain regions associated with negative salience were found to be significant (i.e., increased values in the control group).

Brain Regions	LV1 (negative)		
	TV (Mean ± std)		Salience (Mean ± std)
	HSAM	controls	
HC right	0.97 ± 0.02	0.98 ± 0.01	-0.009 ± 0.003
TempP left	0.94 ± 0.04	0.97 ± 0.02	-0.018 ± 0.009

Left column: TV of controls group; right column: TV of HSAM. Only significant saliences after the bootstrapping are shown. HC: hippocampus; TempP: temporal pole.

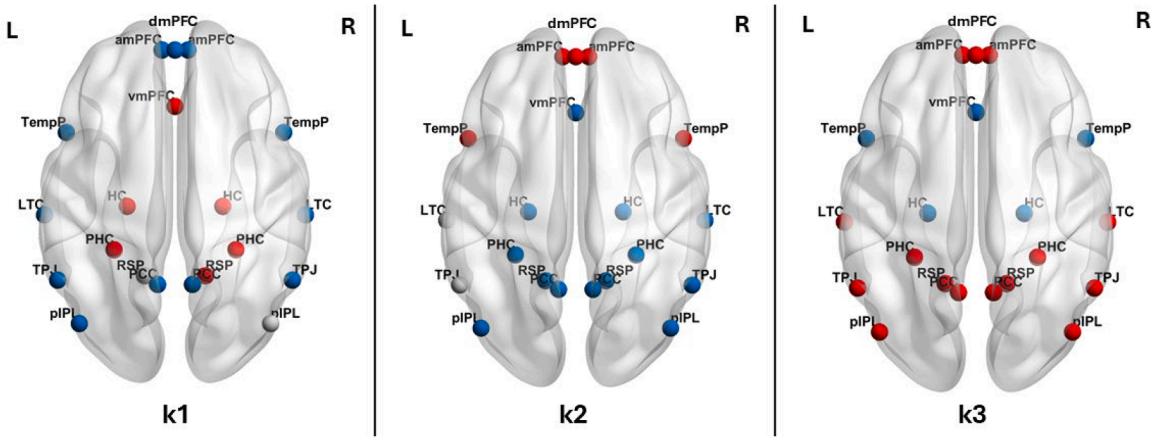

Fig. 4. Axial brain representations of the three brain states identified in the entire HSAM and control subject dataset. From left to right, patterns k1, k2, and k3 are shown. Blue nodes indicate brain regions with positive BOLD signal, red nodes indicate regions with negative BOLD signal, and grey nodes indicate neutral regions. Patterns k1 and k2 show overlapping regions primarily within the dorsal medial and medial temporal subsystems, respectively. Pattern k3 exhibits a mixed pattern involving the hippocampus (HC), temporal pole (TempP), and ventromedial prefrontal cortex (vmPFC). Brain states were estimated using concatenated scans from all subjects, capturing the dynamic properties of the entire dataset.

Table 5
Positive and negative values of each brain regions included in the three clusters.

Cluster (k)	Brain Regions	
	Positive	Negative
1	LTC left and right PCC left and right TPJ left and right TempP left and right amPFC left and right pIPL left dmPFC	HC left and right PHC left and right RSP right vmPFC
2	HC left and right PCC left and right PHC left and right RSP left and right pIPL left and right LTC right TPJ right vmPFC	TempP left and right amPFC left dmPFC
3	HC left and right TempP left and right vmPFC	LTC left and right PCC left and right PHC left and right RSP left and right TPJ left and right amPFC left and right pIPL left and right dmPFC

HSAM and matched controls. By focusing on resting-state DMN connectivity, we characterized task-independent network organization in HSAM relative to controls, within a core brain system supporting autobiographical memory, self-referential cognition, and internally oriented mental activity (Buzsáki and Moser, 2013; Nadel, 2013; Maguire and Mullally, 2013; Moscovitch et al., 2016; Rolls, 2022). Specifically, we examined (A) single-link connectivity, capturing direct interactions between pairs of regions; (B) single-node connectivity, reflecting both overall connection strength and temporal stability of individual nodes; and (C) whole-network connectivity, assessed through CAP analyses, describing large-scale integration and dynamic network states. Across these levels, we tested for differences between HSAM and control participants.

At the single-link level, HSAM individuals exhibited enhanced medial antero-posterior connectivity, particularly among memory-related regions, including the mPFC and vmPFC, the HC and PHC, and extending posteriorly to the RSP. This pattern suggests stronger direct pairwise interactions among key memory-related nodes even during rest (Buzsáki and Moser, 2013; Nadel, 2013; Maguire and Mullally, 2013; Rolls, 2022; Moscovitch et al., 2016). These findings are consistent with previous findings linking synchronized mPFC-HC activity to memory function in both humans and animal models (Liu et al., 2018b; Zielinski et al., 2019; Minxha et al., 2020). Particularly, increased mPFC–HC connectivity in humans has been associated with memory encoding (Zeithamova et al., 2012; van Kesteren et al., 2010; Schlichting and Preston, 2016) and retrieval (Addis et al., 2004; Robin et al., 2015; Bellana et al., 2017; Inman et al., 2018). Evidence from dynamic causal modeling (DCM) analysis has further shown top-down modulation from the prefrontal cortex to the hippocampus during memory reactivation (Fuentemilla et al., 2014; McCormick et al., 2015, 2020; Nawa and Ando, 2019). In parallel with the well-established contribution of the medial temporal lobe to episodic and autobiographical memory (Squire et al., 2004), the vmPFC has been proposed to organize and represent long-term memory through schematic frameworks (Gilboa and Marlatte, 2017). Patients with vmPFC lesions show impaired free recall despite intact cued retrieval (Bertossi et al., 2016; Thaiss and Petrides, 2008), suggesting that this region supports strategic monitoring and schema construction rather than memory storage *per se* (McCormick et al., 2018; Sekeres et al., 2018). This interpretation is consistent with previous task-based fMRI studies in HSAM individuals, which reported increased

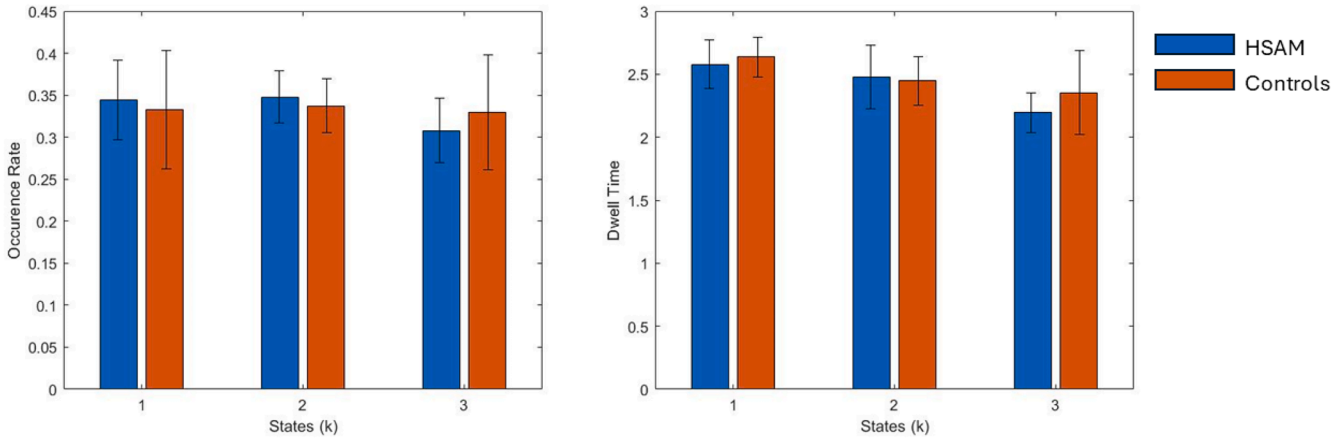

Fig. 5. Dynamical characterization of brain states. Left panel: occurrence rate; right panel; dwell time. Control group in blue; HSAM group in red. No significant results were found for both measures.

Table 6
Mean and standard deviation of occurrence rate and dwell time characterizing both groups.

		1	2	3
HSAM	Occurrence rate	0.33 ± 0.07	0.34 ± 0.03	0.33 ± 0.07
	Dwell time	2.6 ± 0.2	2.4 ± 0.2	2.4 ± 0.3
HC	Occurrence rate	0.34 ± 0.05	0.35 ± 0.03	0.31 ± 0.04
	Dwell time	2.6 ± 0.2	2.5 ± 0.3	2.2 ± 0.2

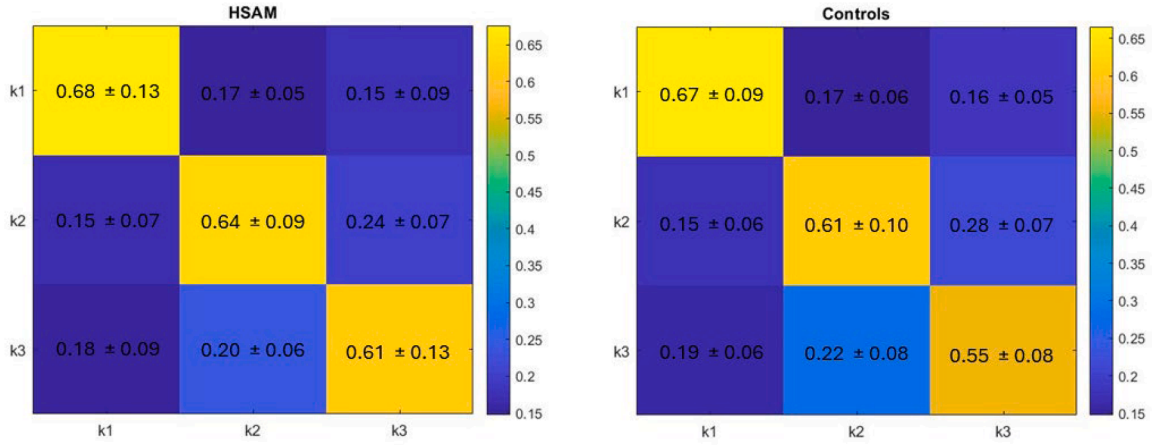

Fig. 6. Transition matrix between brain states (k1, k2, and k3), reporting the mean and the standard deviation of the transition probability for each combination. HSAM and control groups are shown in the left and right panel, respectively.

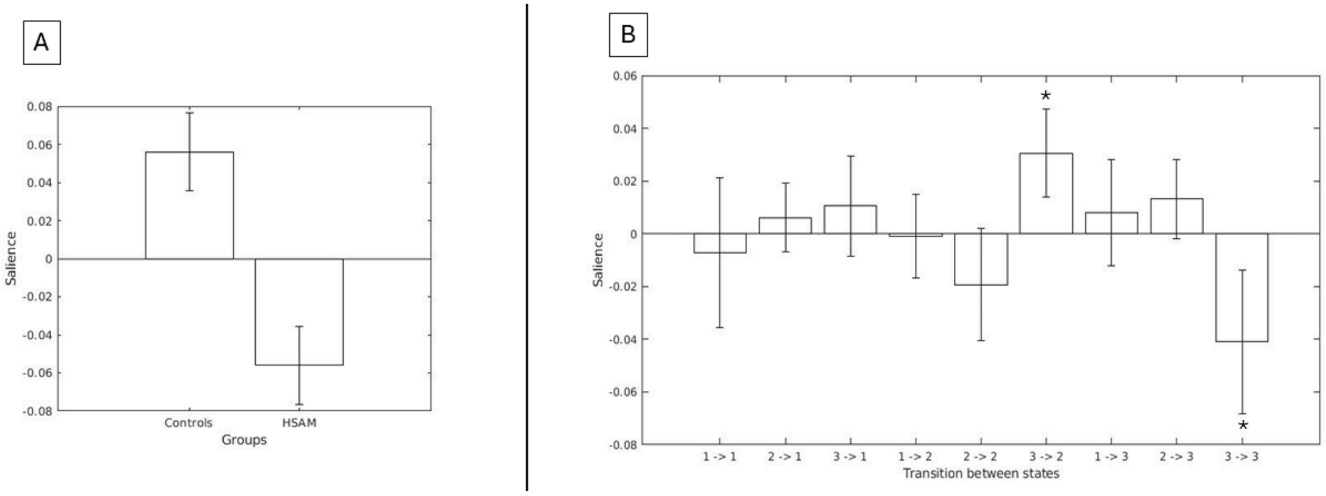

Fig. 7. Saliences of the main Latent Variable (LV), which characterizes an opposite pattern of transition probability between groups. Positive and negative saliences were associated to the controls and HSAM group, respectively. Panel A: saliences of explanatory variables; Panel B: transition probability vectors of salience related to each brain region. Asterisks indicate significant salience after the permutation test. Error bars represent 95% CIs.

vmPFC activation and enhanced medial DMN connectivity—particularly between the vmPFC and the HC— during the construction phase of autobiographical memory retrieval (Santangelo et al., 2018, 2020, 2021). The present findings extend this evidence, showing that this enhanced communication occurs even at rest, possibly reflecting a continuous background state supporting spontaneous memory reactivation or consolidation. Speculatively, this mechanism may represent either a neural precursor or a functional consequence of the superior mnemonic abilities observed in HSAM.

At the nodal level, HSAM individuals exhibited increased node strength in the HC and PHC relative to controls, highlighting the central role of medial temporal lobe components of the DMN in HSAM. In addition, the TempP, together with the HC, showed reduced temporal variability, indicating more stable communication dynamics over time. This region is well known to support autobiographical memory, semantic representation, and emotional processing (Olson et al., 2007) and is particularly involved in integrating newly encoded information with prior knowledge representations. As a general comment on TV analysis, previous studies have linked lower variability at rest with higher general intelligence (Hilger et al., 2020), whereas increased variability during task performance has been associated with greater executive flexibility (Sun et al., 2019). Additionally, DMN variability has been shown to increase following sleep deprivation (Sun et al., 2022), a condition known to impair memory consolidation (Joo and Frank, 2018). These discrepancies likely reflect differences in experimental context: during rest, more stable connectivity may support cognitive performance, whereas during task execution, higher variability may reflect the flexibility required to adapt to dynamically changing stimuli. Accordingly, the reduced temporal variability observed here may indicate a more stable intrinsic network organization that facilitates memory integration and long-term consolidation in HSAM individuals. In summary, reduced variability combined with increased functional connectivity in these regions likely reflects more persistent and coherent information transfer within the DMN (Tognoli and Kelso, 2014; Keilholz et al., 2017) and may serve as a neural signature of continuous rehearsal and consolidation of autobiographical memories (Moscovitch et al., 2016; Sekeres et al., 2018).

At the whole-network level, the CAP analysis identified three distinct clusters. The first two clusters displayed opposing dynamics within DMN subsystems (as described by Andrews-Hanna et al., 2014a): the dorsal medial subsystem and the medial temporal subsystem, respectively for k1 and k2. The third cluster (k3) reflects a distinct circuit involving the HC, vmPFC, and the TempP, a configuration that integrated regions related to memory and self-reference. Group comparisons showed that HSAM participants had a higher self-transition probability for this cluster relative to controls. At the same time, unchanged dwell time and

occurrence rate indicate that this state is more likely to be re-engaged when already active, without being visited more often or for longer overall. In dynamical-systems terms (Kelso, 2012), increased self-transition probability without corresponding changes in dwell time or occurrence reflects greater attractiveness of the state, rather than increased global persistence. It is interesting to note that, from an anatomical perspective, the regions involved in k3 partially overlap with the brain areas connected by the uncinate fasciculus (Von Der Heide et al., 2013). This white-matter pathway has previously been associated with HSAM (LePort et al., 2012), and multimodal MRI studies using both fMRI and DTI analyses have shown that its structural integrity is related to functional activity in the medial temporal gyrus and to the facilitation of autobiographical memory (Memel et al., 2020; Granger et al., 2021), particularly regarding event-element details (Memel et al., 2020). It is worth noting that this brain pattern is also consistent with the anterior hippocampal circuit described by Poppenk et al. (2013) and confirmed by more recent evidence (Angeli et al., 2025), which is characterized by cortical reinstatement of memories and schema formation, as opposed to the posterior hippocampus, which is involved in the detailed reconstruction of memory events. The current results extend these observations, demonstrating enhanced resting-state co-activation among memory- and self-referential regions, potentially reflecting more continuous offline replay and schema-integration processes (Kaefer et al., 2022). Recent theoretical and empirical work has proposed that such enhanced coupling among memory-related and self-referential DMN regions may support neural replay — the spontaneous reactivation of patterns of neural activity associated with previous experiences during rest or quiet wakefulness (Carr et al., 2011; Ritchey and Cooper, 2020; Tambini and Davachi, 2019). Neural replay has been observed in both hippocampal and cortical areas and is thought to facilitate the transfer and integration of memory traces from the hippocampus to neocortical networks (McClelland et al., 1995; Klinzing et al., 2019). Within this framework, the increased resting-state connectivity and stability of this brain state in HSAM could reflect an enhanced capacity for spontaneous reactivation and consolidation of autobiographical information. In particular, the vmPFC-HC circuit could be involved in the coordination of replay events that support the abstraction of general knowledge structures, while the TempP contributes to schema-based memory retrieval (Irish et al., 2012; Miller-Goldwater et al., 2021). Therefore, the enhanced and temporally stable communication we observed between these regions in the HSAM may reflect a neural substrate that enables the continuous integration of novel experiences into richly detailed autobiographical memory networks.

5. Conclusion

Taken together, our findings converge toward a coherent picture of enhanced DMN connectivity in HSAM individuals across single-link (A), node (B), and whole-network (C) levels. The most pronounced effects involved stronger and more stable communication between memory-related regions such as the HC and PHC, and self-referential regions including the vmPFC. This pattern suggests that HSAM is associated with a highly integrated and temporally stable DMN architecture that may facilitate the continuous consolidation and integration of autobiographical experiences. Enhanced mPFC–HC coupling, in particular, may support the incorporation of new memories into existing self-related schemas, promoting vivid and enduring autobiographical recollection.

Data and code availability statement

The datasets generated and analyzed during the current study are not publicly available due to institutional restrictions. Requests for access to the data can be directed to the corresponding author and will be considered on a case-by-case basis.

All custom scripts employed for data processing, analysis, and visualization are available from the corresponding author upon reasonable request.

CRediT authorship contribution statement

Fabrizio Parente: Writing – original draft, Formal analysis, Data curation. **Tiziana Pedale:** Writing – review & editing, Investigation, Data curation, Conceptualization. **Ilenia Salsano:** Writing – review & editing. **Patrizia Campolongo:** Writing – review & editing, Funding acquisition, Conceptualization. **Valerio Santangelo:** Writing – review & editing, Supervision, Funding acquisition, Conceptualization.

Declaration of competing interest

Research Support

Valerio Santangelo and Patrizia Campolongo reports financial support was provided by Italian Ministry of University and Research (grant number: J53D23017260001).

Relationship

There are no additional relationships to disclose.

Patents and Intellectual Property

There are no patents to disclose.

Other Activities

There are no additional activities to disclose.

Acknowledgments

Supported by the European Union -NextGenerationEU- Italian Ministry of University and Research (MUR), National Plan for Recovery and Resilience (NRRP) and Projects of National Relevance (PRIN), Project Code: P2022LX894, CUP: J53D23017260001, awarded to V.S. and P.C.

References

Addis, D.R., McIntosh, A.R., Moscovitch, M., Crawley, A.P., McAndrews, M.P., 2004. Characterizing spatial and temporal features of autobiographical memory retrieval networks: a partial least squares approach. Neuroimage 23 (4), 1460–1471.
Ally, B.A., Hussey, E.P., Donahue, M.J., 2013. A case of hyperthymesia: rethinking the role of the amygdala in autobiographical memory. Neurocase 19 (2), 166–181.
Andrews-Hanna, J.R., Reidler, J.S., Sepulcre, J., Poulin, R., Buckner, R.L., 2010. Functionalanatomic fractionation of the brain's default network. Neuron 65 (4), 550–562.
Andrews-Hanna, J.R., Saxe, R., Yarkoni, T., 2014a. Contributions of episodic retrieval and mentalizing to autobiographical thought: Evidence from functional neuroimaging, restingstate connectivity, and fMRI metaanalyses. Neuroimage 91, 324–335.
Andrews-Hanna, J.R., Smallwood, J., Spreng, R.N., 2014b. The default network and selfgenerated thought: component processes, dynamic control, and clinical relevance. Ann. N. Y. Acad. Sci. 1316 (1), 29–52.
Angeli, P.A., DiNicola, L.M., Saadon-Grosman, N., Eldaief, M.C., Buckner, R.L., 2025. Specialization of the human hippocampal long axis revisited. Proc. Natl. Acad. Sci. U. S. A. 122 (3), e2422083122.
Bellana, B., Liu, Z.X., Diamond, N.B., Grady, C.L., Moscovitch, M., 2017. Similarities and differences in the default mode network across rest, retrieval, and future imagining. Hum. Brain Mapp. 38 (3), 1155–1171.
Behzadi, Y., Restom, K., Liau, J., Liu, T.T., 2007. A componentbased noise correction method (CompCor) for BOLD and perfusion based fMRI. Neuroimage 37 (1), 90–101.
Bertossi, E., Tesini, C., Cappelli, A., Ciaramelli, E., 2016. Ventromedial prefrontal damage causes a pervasive impairment of episodic memory and future thinking. Neuropsychologia 81, 107e116.
Betzel, R.F., Faskowitz, J., Sporns, O., 2023. Living on the edge: network neuroscience beyond nodes. Trends Cogn. Sci. 27 (11), 1068–1084.
Binder, J.R., Desai, R.H., 2011. The neurobiology of semantic memory. Trends Cogn. Sci. 15 (11), 527–536.
Borgatti, S.P., Everett, M.G., 2006. A graphtheoretic perspective on centrality. Soc. Netwo. 28, 466–484.
Brandt, J., Bakker, A., 2018. Neuropsychological investigation of "The amazing memory man. Neuropsychology 32 (3), 304–316.
Buckner, R.L., Carroll, D.C., 2007. Selfprojection and the brain. Trends Cogn. Sci. 11 (2), 49–57.
Buzsáki, G., Moser, E.I., 2013. Memory, navigation and theta rhythm in the hippocampalentorhinal system. Nat. Neurosci. 16 (2), 130–138.
Caliński, T., Harabasz, J., 1974. A dendrite method for cluster analysis. Commun. Stat. 3 (1), 1–27.

Chai, X.J., Castañón, A.N., Öngür, D., WhitfieldGabrieli, S., 2012. Anticorrelations in resting state networks without global signal regression. Neuroimage 59 (2), 1420–1428.
Chang, C., Glover, G.H., 2009. Effects of modelbased physiological noise correction on default mode network anticorrelations and correlations. Neuroimage 47 (4), 1448–1459.
Carr, M.F., Jadhav, S.P., Frank, L.M., 2011. Hippocampal replay in the awake state: a potential substrate for memory consolidation and retrieval. Nat. Neurosci. 14, 147–153.
Daviddi, S., Orwig, W., Palmiero, M., Campolongo, P., Schacter, D.L., Santangelo, V., 2022a. Individuals with highly superior autobiographical memory do not show enhanced creative thinking. Memory 30 (9), 1148–1157.
Daviddi, S., Pedale, T., Serra, L., Macrì, S., Campolongo, P., Santangelo, V., 2022b. Altered hippocampal restingstate functional connectivity in highly superior autobiographical memory. Neuroscience 480, 1–8.
Daviddi, S., Pedale, T., St Jacques, P.L., Schacter, D.L., Santangelo, V., 2023. Common and distinct correlates of construction and elaboration of episodic-autobiographical memory: an ALE meta-analysis. Cortex 163, 123–138.
Daviddi, S., Yaya, G., Sperduti, M., Santangelo, V., 2024. A systematic review and meta-analysis of the neural correlates of direct vs. generative retrieval of episodic autobiographical memory. Neuropsychol. Rev. advance online publication.
De Marco, M., Mazzoni, G., Manca, R., Venneri, A., 2021. Functional neural architecture supporting highly superior autobiographical memory. Brain Connect. 11 (4), 297–307.
Efron, B., Tibshirani, R., 1986. Bootstrap methods for standard errors, confidence intervals, and other measures of statistical accuracy. Stat. Sci. 1, 54–75.
Ford, L., Shaw, T.B., Mattingley, J.B., Robinson, G.A., 2022. Enhanced semantic memory in a case of highly superior autobiographical memory. Cortex 151, 1–14.
Fox, M.D., Zhang, D., Snyder, A.Z., Raichle, M.E., 2009. The global signal and observed anticorrelated resting state brain networks. J. Neurophysiol. 101 (6), 3270–3283.
Fuentemilla, L., Barnes, G.R., Düzel, E., Levine, B., 2014. Theta oscillations orchestrate medial temporal lobe and neocortex in remembering autobiographical memories. Neuroimage 85 (Pt 2), 730–737.
Gibson, E.C., Ford, L., Robinson, G.A., 2022. Investigating the role of future thinking in a case of highly superior autobiographical memory. Cortex 149, 188–201.
Gilboa, A., Marlatte, H., 2017. Neurobiology of schemas and schema-mediated memory. Trends Cogn. Sci. 21 (8), 618–631.
Gopinath, K., Krishnamurthy, V., Cabanban, R., Crosson, B., 2015. Hubs of anticorrelation in highresolution restingstate functional connectivity network architecture. Brain Connect. 5 (5), 267–275.
Granger, S.J., Leal, S.L., Larson, M.S., Janecek, J.T., McMillan, L., Stern, H., Yassa, M.A., 2021. Integrity of the uncinate fasciculus is associated with emotional pattern separation-related fMRI signals in the hippocampal dentate and CA3. Neurobiol. Learn. Mem. 177, 107359.
Greicius, M.D., Supekar, K., Menon, V., Dougherty, R.F., 2009. Resting state functional connectivity reflects structural connectivity in the default mode network. Cereb. Cortex 19, 72–78.
Hassabis, D., Maguire, E.A., 2009. The construction system of the brain. Philos. Trans. R. Soc. B Biol. Sci. 364 (1521), 1263–1271.
Hilger, K., Fukushima, M., Sporns, O., Fiebach, C.J., 2020. Temporal stability of functional brain modules associated with human intelligence. Hum. Brain Mapp. 41 (2), 362–372.
Inman, C.S., James, G.A., Vytal, K., Hamann, S., 2018. Dynamic changes in largescale functional network organization during autobiographical memory retrieval. Neuropsychologia 110, 208–224.
Irish, M., Addis, D.R., Hodges, J.R., Piguet, O., 2012. Considering the role of semantic memory in episodic future thinking: evidence from semantic dementia. Brain 135 (7), 2178–2191.
Joo, H.R., Frank, L., 2018. The hippocampal sharp waveripple in memory retrieval for immediate use and consolidation. Nat. Rev. Neurosci. 19 (12), 744–757.
Kaefer, K., Stella, F., McNaughton, B.L., Battaglia, F.P., 2022. Replay, the default mode network and the cascaded memory systems model. Nat. Rev. Neurosci. 23 (10), 628–640.
Keilholz, S., CaballeroGaudes, C., Bandettini, P., Deco, G., Calhoun, V., 2017. Timeresolved restingstate functional magnetic resonance imaging analysis: current status, challenges, and new directions. Brain Connect. 7 (8), 465–481.
Kelso, J.A., 2012. Multistability and metastability: understanding dynamic coordination in the brain. Philos. Trans. R. Soc. Lond. B Biol. Sci. 367 (1591), 906–918.
Kim, H.C., Lee, J.H., 2022. Spectral dynamic causal modeling of mindfulness, mindwandering, and resting state in the triple network using fMRI. Neuroreport 33 (5), 221–226.
Klinzing, J.G., Niethard, N., Born, J., 2019. Mechanisms of systems memory consolidation during sleep. Nat. Neurosci. 22, 1598–1610.
Krishnan, A., Williams, L.J., McIntosh, A.R., Abdi, H., 2011. Partial least squares (PLS) methods for neuroimaging: a tutorial and review. Neuroimage 56, 455–475.
LePort, A.K.R., Mattfeld, A.T., DickinsonAnson, H., Fallon, J.H., Stark, C.E.L., Kruggel, F., Cahill, L., McGaugh, J.L., 2012. Behavioral and neuroanatomical investigation of highly superior autobiographical memory (HSAM). Neurobiol. Learn. Mem. 98 (1), 78–92.
LePort, A.K., Stark, S.M., McGaugh, J.L., Stark, C.E., 2017. A cognitive assessment of highly superior autobiographical memory. Memory 25, 276–288.
Liu, X., Chang, C., Duyn, J.H., 2013. Decomposition of spontaneous brain activity into distinct fMRI coactivation patterns. Front. Syst. Neurosci. 7, 101.
Liu, X., Zhang, N., Chang, C., Duyn, J.H., 2018a. Coactivation patterns in restingstate fMRI signals. Neuroimage 180 (Pt B), 485–494.
Liu, T., Bai, W., Xia, M., Tian, X., 2018b. Directional hippocampalprefrontal interactions during working memory. Behav. Brain Res. 338, 1–8.
Long, Y., Liu, X., Liu, Z., 2023. Temporal stability of the dynamic restingstate functional brain network: current measures, clinical research progress, and future perspectives. Brain Sci. 13 (3), 429.
Maguire, E.A., Mullally, S.L., 2013. The hippocampus: a manifesto for change. J. Exp. Psychol. Gen. 142 (4), 1180–1189.
Mazzoni, G., Clark, A., De Bartolo, A., Guerrini, C., Nahouli, Z., Duzzi, D., De Marco, M., McGeown, W., Venneri, A., 2019. Brain activation in highly superior autobiographical memory: the role of the precuneus in the autobiographical memory retrieval network. Cortex 120, 588–602.
McClelland, J.L., McNaughton, B.L., O'Reilly, R.C., 1995. Why there are complementary learning systems in the hippocampus and neocortex: insights from the successes and failures of connectionist models of learning and memory. Psychol. Rev. 102 (3), 419–457.
McCormick, C., StLaurent, M., Ty, A., Valiante, T.A., McAndrews, M.P., 2015. Functional and effective hippocampalneocortical connectivity during construction and elaboration of autobiographical memory retrieval. Cereb. Cortex 25 (5), 1297–1305.
McCormick, C., Barry, D.N., Jafarian, A., Barnes, G.R., Maguire, E.A., 2020. vmPFC drives hippocampal processing during autobiographical memory recall regardless of remoteness. Cereb. Cortex 30 (11), 5972–5987.
McCormick, C., Ciaramelli, E., De Luca, F., Maguire, E.A., 2018. Comparing and contrasting the cognitive effects of hippocampal and ventromedial prefrontal cortex damage: a review of human lesion studies. Neuroscience 374, 295–318.
McIntosh, A.R., Lobaugh, N.J., 2004. Partial least squares analysis of neuroimaging data: applications and advances. Neuroimage 23 (1), S250–S263.
Memel, M., Wank, A.A., Ryan, L., Grilli, M.D., 2020. The relationship between episodic detail generation and anterotemporal, posteromedial, and hippocampal white matter tracts. Cortex 123, 124–140.
Menon, B., 2019. Towards a new model of understanding – the triple network, psychopathology and the structure of the mind. Med. Hypotheses 133, 109385.
MillerGoldwater, H.E., CroninGolomb, L.M., Porter, B.M., Bauer, P.J., 2021. Developmental differences in reactivation underlying selfderivation of new knowledge through memory integration. Cogn. Psychol. 129, 101413.
Minxha, J., Adolphs, R., Fusi, S., Mamelak, A.N., Rutishauser, U., 2020. Flexible recruitment of memorybased choice representations by the human medial frontal cortex. Science 368, eaba3313 (1979).
Moscovitch, M., Cabeza, R., Winocur, G., Nadel, L., 2016. Episodic memory and beyond: the hippocampus and neocortex in transformation. Annu. Rev. Psychol. 67, 105–134.
Murphy, R., Birn, R., Handwerker, D., Jones, T., Bandettini, P., 2009. The impact of global signal regression on resting state correlations: Are anticorrelated networks introduced? Neuroimage 44 (1), 893–905.
Nadel, L., Hoscheidt, S., Ryan, L.R., 2013. Spatial cognition and the hippocampus: the anteriorposterior axis. J. Cogn. Neurosci. 25 (1), 22–28.
Nawa, N.E., Ando, H., 2019. Effective connectivity within the ventromedial prefrontal cortexhippocampusamygdala network during the elaboration of emotional autobiographical memories. Neuroimage 189, 316–328.
Olson, I.R., Plotzker, A., Ezzyat, Y., 2007. The enigmatic temporal pole: a review of findings on social and emotional processing. Brain 130 (Pt 7), 1718–1731.
Orwig, W., Diez, I., Bueichekú, E., et al., 2024. Cortical hubs of highly superior autobiographical memory. Cortex 179, 14–24.
Palombo, D.J., Sheldon, S., Levine, B., 2018. Individual differences in autobiographical memory. Trends Cogn. Sci. 22 (7), 583–597.
Parente, F., Colosimo, A., 2020. Functional connections between and within brain subnetworks under resting state. Sci. Rep. 10 (1), 3438.
Parker, E.S., Cahill, L., McGaugh, J.L., 2006. A case of unusual autobiographical remembering. Neurocase 12, 35–49.
Patihis, L., Frenda, S.J., LePort, A.K., Petersen, N., Nichols, R.M., Stark, C.E., McGaugh, J. L., Loftus, E.F., 2013. False memories in highly superior autobiographical memory individuals. Proc. Natl. Acad. Sci. U. S. A. 110 (52), 20947–20952.
Poppenk, J., Evensmoen, H.R., Moscovitch, M., Nadel, L., 2013. Long-axis specialization of the human hippocampus. Trends Cogn Sci. 17 (5), 230–240.
Power, J.D., Mitra, A., Laumann, T.O., Snyder, A.Z., Schlaggar, B.L., Petersen, S.E., 2014. Methods to detect, characterize, and remove motion artifact in resting state fMRI. Neuroimage 84, 320–341.
Rubinov, M., Sporns, O., 2010. Complex network measures of brain connectivity: uses and interpretations. Neuroimage 52 (3), 1059–1069.
Raichle, M.E., MacLeod, A.M., Snyder, A.Z., Powers, W.J., Gusnard, D.A., Shulman, G.L., 2001. A default mode of brain function. Proc. Natl. Acad. Sci. U. S. A. 98, 676–682.
Raichle, M.E., Snyder, A.Z., 2007. A default mode of brain function: a brief history of an evolving idea. Neuroimage 37, 1083–1090.
Ritchey, M., Cooper, R.A., 2020. Deconstructing the posterior medial episodic network. Trends Cogn. Sci. 24 (6), 451–465.
Robin, J., Hirshhorn, M., Rosenbaum, R.S., Winocur, G., Moscovitch, M., Grady, C.L., 2015. Functional connectivity of hippocampal and prefrontal networks during episodic and spatial memory based on realworld environments. Hippocampus 25 (1), 81–93.
Rolls, E.T., 2022. The hippocampus, ventromedial prefrontal cortex, and episodic and semantic memory. Prog. Neurobiol. 217, 102334.
Santangelo, V., Cavallina, C., Colucci, P., et al., 2018. Enhanced brain activity associated with memory access in highly superior autobiographical memory. Proc. Natl. Acad. Sci. U. S. A. 115 (30), 7795–7800.
Santangelo, V., Pedale, T., Macrì, S., Campolongo, P., 2020. Enhanced cortical specialization to distinguish older and newer memories in highly superior autobiographical memory. Cortex 129, 476–483.

Santangelo, V., Pedale, T., Colucci, P., Giulietti, G., Macrì, S., Campolongo, P., 2021. Highly superior autobiographical memory in aging: a single case study. Cortex 143, 267–280.
Santangelo, V., Macrì, S., Campolongo, P., 2022. Superior memory as a new perspective to tackle memory loss. Neurosci. Biobehav. Rev. 141, 104828.
Santangelo, V., Pedale, T., Daviddi, S., Salsano, I., Macrì, S., Campolongo, P., 2025. Altered brain activity during active forgetting in highly superior autobiographical memory: evidence from an item-method directed forgetting. iScience 28 (6), 112607.
Schlichting, M.L., Preston, A.R., 2016. Hippocampalmedial prefrontal circuit supports memory updating during learning and postencoding rest. Neurobiol. Learn. Mem. 134, 91–106.
Sekeres, M.J., Winocur, G., Moscovitch, M., 2018. The hippocampus and related neocortical structures in memory transformation. Neurosci. Lett. 680, 39–53.
Shmuel, A., Yacoub, E., Pfeuffer, J., et al., 2002. Sustained negative BOLD, blood flow and oxygen consumption response and its coupling to the positive response in the human brain. Neuron 36 (6), 1195–1210.
Spreng, R.N., Mar, R.A., Kim, A.S., 2009. The common neural basis of autobiographical memory, prospection, navigation, theory of mind, and the default mode: a quantitative metaanalysis. J. Cogn. Neurosci. 21 (3), 489–510.
Squire, L.R., Stark, C.E., Clark, R.E., 2004. The medial temporal lobe. Annu. Rev. Neurosci. 27, 279–306.
Sun, J., Liu, Z., Rolls, E.T., et al., 2019. Verbal creativity correlates with the temporal variability of brain networks during the resting state. Cereb. Cortex 29 (3), 1047–1058.
Sun, J., Zhao, R., He, Z., Chang, M., Wang, F., Wei, W., Zhang, X., Zhu, Y., Xi, Y., Yang, X., Qin, W., 2022. Abnormal dynamic functional connectivity after sleep deprivation from temporal variability perspective. Hum. Brain Mapp. 43 (12), 3824–3839.
Talbot, J., Convertino, G., De Marco, M., Venneri, A., Mazzoni, G., 2025. Highly superior autobiographical memory (HSAM): a systematic review. Neuropsychol. Rev. 35 (1), 54–76.
Tambini, A., Davachi, L., 2019. Awake reactivation of prior experiences consolidates memories and biases cognition. Trends Cogn. Sci. 23 (10), 876–890.
Taylor, A.J., Kim, J.H., Ress, D., 2022. Temporal stability of the hemodynamic response function across the majority of human cerebral cortex. Hum. Brain Mapp. 43 (16), 4924–4942.
Thaiss, L., Petrides, M., 2008. Autobiographical memory of the recent past following frontal cortex or temporal lobe excisions. Eur. J. Cogn. Psychol. 28 (4), 829–840.
Tognoli, E., Kelso, J.A., 2014. The metastable brain. Neuron 81 (1), 35–48.
Von Der Heide, R.J, Skipper, L.M, Klobusicky, E., Olson, I.R., 2013. Dissecting the uncinate fasciculus: disorders, controversies and a hypothesis. Brain 136 (Pt 6), 1692–1707.
Van Kesteren, M.T., Fernandez, G., Norris, D.G., Hermans, E.J., 2010. Persistent schemadependent hippocampalneocortical connectivity during memory encoding and postencoding rest in humans. Proc. Natl. Acad. Sci. U. S. A. 107, 7550–7555.
WhitfieldGabrieli, S., NietoCastañón, A., 2012. Conn: a functional connectivity toolbox for correlated and anticorrelated brain networks. Brain Connect. 2 (3), 125–141.
Zeithamova, D., Dominick, A.L., Preston, A.R., 2012. Hippocampal and ventral medial prefrontal activation during retrievalmediated learning supports novel inference. Neuron 75, 168–179.
Zhang, J., Cheng, W., Liu, Z., Zhang, K., Lei, X., Yao, Y., Becker, B., Liu, Y., Kendrick, K. M., Lu, G., et al., 2016. Neural, electrophysiological and anatomical basis of brainnetwork variability and its characteristic changes in mental disorders. Brain 139, 2307–2321.
Zhou, X., Lei, X., 2018. Wandering minds with wandering brain networks. Neurosci. Bull. 34 (6), 1017–1028.
Zielinski, M.C., Shin, J.D., Jadhav, S.P., 2019. Coherent coding of spatial position mediated by theta oscillations in the hippocampus and prefrontal cortex. J. Neurosci. 39, 4550–4565.